Synthesizing Weyl semimetals in weak topological insulator and topological crystalline insulator multilayers

Alexander Lau[1] and Carmine Ortix[1,2]

[1]*Institute for Theoretical Solid State Physics, IFW Dresden, 01171 Dresden, Germany*

[2]*Institute for Theoretical Physics, Center for Extreme Matter and Emergent Phenomena,
Utrecht University, Princetonplein 5, 3584 CC Utrecht, Netherlands*

We propose a different route to time-reversal invariant Weyl semimetals by employing multilayer heterostructures comprising ordinary "trivial" insulators and nontrivial insulators with *pairs* of protected Dirac cones on the surface. We consider both the case of weak topological insulators, where surface Dirac cones are pinned to time-reversal invariant momenta, and of topological crystalline insulators with unpinned surface Dirac cones. For both realizations we explain phenomenologically how the proposed construction leads to the emergence of a Weyl semimetal phase. We further formulate effective low-energy models for which we prove the existence of semimetallic phases with four isolated Weyl points. Finally, we discuss how the proposed design can be realized experimentally with state-of-the-art technologies.

Introduction. Topological phases are novel states of matter whose study has led to a plethora of fascinating discoveries and developments in modern condensed-matter physics [1–11]. In gapped systems, the quantized invariant of a topological quantum state of matter is directly related to the presence of protected edge or surface states by the so-called bulk-boundary correspondence [1,2]. The most famous examples of topological materials are two-dimensional (2D) and three-dimensional (3D) time-reversal invariant (TRI) topological insulators (TIs) [12–20], as well as topological crystalline insulators (TCIs) [21–26].

Weyl semimetals (WSMs), instead, are members of the family of *gapless* topological phases [7,27–29], and have recently been discovered experimentally [30–36]. WSMs are 3D materials whose bulk energy bands cross linearly at isolated points in the Brillouin zone (BZ), the so-called Weyl nodes [37–40]. Around these points the system can be effectively described by a Weyl Hamiltonian of the general form $H(\mathbf{k}) = \sum_{ij} k_i A_{ij} \sigma_j$, where $i = x,y,z$, $j = 0,x,y,z$, and σ_j are Pauli matrices [41]. A necessary condition for a WSM is the absence of either time-reversal or inversion symmetry since the simultaneous presence of both requires any band crossing to be at least a fourfold degenerate Dirac point.

Weyl nodes represent monopoles of the Berry flux in momentum space, and can be assigned a well-defined chirality or topological charge. They always come in pairs of opposite chirality due to the charge neutrality of the BZ. Moreover, in the case of TRI Weyl semimetals, the minimal number of Weyl points is four since time reversal always connects Weyl points with the same chirality. Perturbations can merely shift the nodes in energy or momentum. Therefore, Weyl points are stable bulk features [38,42]. Furthermore, WSMs host robust surface states, commonly referred to as Fermi arcs, connecting Weyl points with opposite topological charge [37,43]. In addition, it has been shown recently that these characteristic arc features can coexist with topological Dirac cones on the surface of a Weyl semimetal [43–45].

In this Rapid Communication, we present a multilayer design for a TRI Weyl semimetal. Multilayer heterostructures

have been proposed for inversion-symmetric [38] and also for time-reversal symmetric WSMs [46], but only considering strong TIs with a single Dirac cone per surface as the active layer. We extend this principle to topological materials with an even number of surface Dirac cones. In particular, we consider two distinct cases: multilayers based on weak TIs with two Dirac cones pinned to TRI momenta, and multilayers based on TCIs with two unpinned Dirac cones. We show that both systems give rise to TRI Weyl semimetal phases with four isolated Weyl nodes. We also find strong TI and weak TI phases in the multilayer phase diagrams, which render the proposed designs a suitable platform for the artificial synthesis of 3D TIs. Moreover, we discuss the experimental feasibility of our theoretical proposal.

Weak TI multilayer. TRI topological insulators are realizations of nontrivial topological phases in the Altland Zirnbauer class AII [47–49]. In three dimensions, gapped systems belonging to this class can be characterized by the four $\mathbb{Z}_2$ topological invariants $\nu_0; (\nu_1 \nu_2 \nu_3)$ [13,50]. Insulators with nonzero ν_0 are called strong TIs. Their hallmark is the existence of an odd number of protected surface Dirac cones *pinned* to TRI momenta [13].

If the strong index ν_0 is zero but at least one of the weak indices ν_1, ν_2, ν_3 is nonzero, the system is dubbed a weak TI. In contrast to their strong relatives, weak TIs feature an even number of topologically protected, *pinned* Dirac cones only at certain surfaces [13,51]. More specifically, there exist so-called "dark surfaces" where surface Dirac cones are absent. These are the surfaces whose Miller indices (modulo 2) are identical to the weak indices $(\nu_1 \nu_2 \nu_3)$. This property is related to the fact that a weak TI is topologically equivalent to a stack of 2D TIs with stacking direction $[\nu_1 \nu_2 \nu_3]$.

Let us now consider a heterostructure consisting of layers of weak TIs as illustrated in Fig. 1(a). Without loss of generality, we consider the invariants of the weak TIs to be 0; (100), i.e., the weak TIs are equivalent to 2D TIs stacked in the x direction, which thus corresponds to the "dark direction." Next, we create a one-dimensional superlattice in the z direction, which is perpendicular to the dark direction, by inserting spacers of
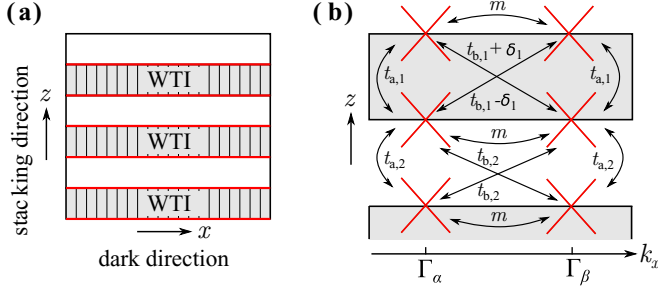
(a)

(b)

FIG. 1. Weak TI multilayer: (a) Cartoon of the multilayer design. The surfaces of the weak TI layers, which contribute two pinned Dirac cones each, are highlighted in red. The layered structure of the weak TIs is indicated. (b) Schematic of the coupling terms between the surface Dirac cones (red). The Dirac cones are pinned to different TRI momenta Γ_α and Γ_β which are mapped onto each other by translational-symmetry breaking induced by the dimerization mass m.

(a) $\delta_1 = 0$
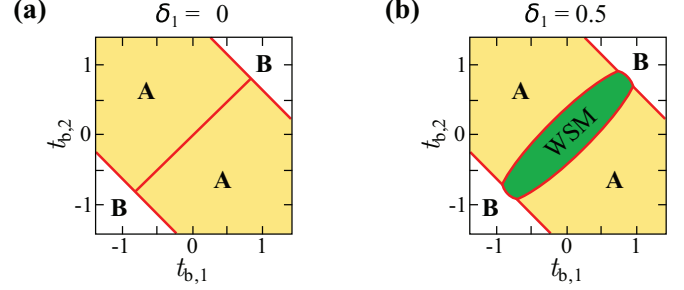

(b) $\delta_1 = 0.5$

FIG. 2. Phase diagrams of the weak TI multilayer with $v_D = m = t_{a,1} = t_{a,2} = 1$. (a) With inversion symmetry ($\delta_1 = 0$): There are two different gapped phases, phase A (strong TI) and phase B (OI), and an unstable Dirac semimetal phase (red lines). (b) Broken inversion symmetry ($\delta_1 = 0.5$): Between the strong TI phases, a stable WSM phase (green) with four separate Weyl points emerges.

ordinary insulators (OIs) between the weak TI layers. Due to the bulk-boundary correspondence, there will be an even number of Dirac cones at each interface between the OI and the weak TI. For simplicity, here we assume each interface to have the minimal number of two Dirac cones. Initially, the Dirac cones are pinned to *different* TRI momenta Γ_α and Γ_β along the dark direction. However, a dimerization in the weak TI crystal [52] breaks the translational symmetry in the dark direction x and allows the two Dirac cones to couple. Furthermore, if weak TI layers and spacer layers are sufficiently thin, also Dirac states from adjacent surfaces can couple through hybridization.

The low-energy theory of the multilayer heterostructure is then effectively described by the following Hamiltonian,

$$
\begin{aligned}
\mathcal{H} = \sum_{\mathbf{k}_\perp, ij} \Big[& v_D \sigma^3 \tau^0 (\hat{z} \times \mathbf{s}) \cdot \mathbf{k}_\perp \, \delta_{i,j} + m \sigma^0 \tau^2 s^3 \, \delta_{i,j} \\
& + t_{a,1} \sigma^1 \tau^0 s^0 \, \delta_{i,j} + \frac{t_{a,2}}{2} (\sigma^- \delta_{i,j+1} + \sigma^+ \delta_{i,j-1}) \tau^0 s^0 \\
& + t_{b,1} \sigma^1 \tau^1 s^0 \, \delta_{i,j} + \delta_1 \sigma^2 \tau^2 s^0 \, \delta_{i,j} \\
& + \frac{t_{b,2}}{2} (\sigma^- \delta_{i,j+1} + \sigma^+ \delta_{i,j-1}) \tau^1 s^0 \Big] c_{\mathbf{k}_\perp, j}^\dagger c_{\mathbf{k}_\perp, i}, \quad (1)
\end{aligned}
$$

where σ^ν, τ^ν, and s^ν are Pauli matrices associated with the top and bottom surfaces of the weak TIs, the two Dirac cones per surface, and the spin degree of freedom, respectively. In addition, v_D is the Fermi velocity of the Dirac fermions, $\mathbf{k}_\perp = (k_x, k_y)$ is their momentum in the 2D surface BZ of the weak TIs, m is the "dimerization mass", and the indices i, j label the weak TI layers. The parameters of our model are illustrated in Fig. 1(b). Note that we also allow for an intervalley coupling imbalance δ_1. Such an imbalance is expected to arise naturally when the top and bottom surfaces of weak TI layers are nonidentical, e.g., when one surface is canted relative to the other. For simplicity, other imbalances have been omitted since they do not change our results qualitatively.

The model of Eq. (1) preserves time-reversal symmetry with the operator $\Theta = i\sigma^0 \tau^0 s^2 K$, $\mathbf{k} \to -\mathbf{k}$, where K is the complex conjugation. The intervalley coupling imbalance serves as an inversion-symmetry breaking term. The corre-

sponding inversion operator is $P = \sigma^1 \tau^0 s^0$, with $\mathbf{k} \to -\mathbf{k}$. In order to pin down the existence of a WSM phase in our model, we compute the energies and monitor the half-filling gap of the system in its parameter space. This allows us to identify gap closing points and their degeneracies. We can anticipate the existence of a WSM phase qualitatively using the following arguments: The hybridization of the surface Dirac cones $\propto t_{a,1}, t_{a,2}$ leads to two 3D Dirac points in the 3D BZ of the model. The dimerization $\propto m$ can either gap out these degeneracy points, leading to fully gapped phases, or shift the two 3D Dirac points in momentum space. Such an unstable Dirac semimetal phase can in principle be transformed into a stable WSM phase by breaking inversion symmetry [38–40]. This is accomplished by the intervalley coupling imbalance: Each 3D Dirac point is split into two separate Weyl points.

Let us first explore the half-filling phase diagram for the inversion-symmetric model with $\delta_1 = 0$ [see Fig. 2(a)]. We find several gapped phases, which we dub A and B, separated by phase boundaries along which the system is semimetallic. More specifically, in the semimetallic phase the system exhibits two unpinned 3D Dirac points on the k_z axis related by time-reversal symmetry.

By exploring the parameter space of our model, we find that the B phases are adiabatically connected to a multilayer of fully decoupled dimerized weak TIs. Since a dimerized weak TI is topologically trivial, these phases correspond to an ordinary insulator with $\mathbb{Z}_2$ invariants $0; (000)$. In order to determine the nature of the other gapped phases, we calculate the corresponding parity eigenvalues of all occupied states at the TRI momenta $\Gamma = (0,0,0)$ and $Z = (0,0,\pi)$ [53], assuming that the topologically active band inversions occur only at these momenta. We find that a band inversion at the Γ point occurs by moving from a B phase to an A phase. On the contrary, no band inversion occurs between the two A phases. Hence, under our assumption, we deduce that the A phases correspond to strong TIs with $\mathbb{Z}_2$ invariants $1; (000)$. We have confirmed these findings by analyzing a lattice regularization of our model (see Ref. [54]).

Let us now turn to the inversion-broken case ($\delta_1 \neq 0$). With inversion symmetry, the two strong TI phases were separated by a Dirac semimetal line. By breaking inversion symmetry, the Dirac points are split into four separate Weyl points along

the k_z axis. In this way, a WSM stability region emerges in the phase diagram [Fig. 2(b)]. By integrating the Berry curvature over a closed momentum-space surface around each of the Weyl nodes, we calculate their topological charges to be ± 1.

In order to synthesize our proposed weak TI multilayer, one could start out with a dimerized weak TI material, namely, $Bi_{13}Pt_3I_7$ [19]. One could then carve an array of sufficiently thin channels into the dark surface of the material, where the channels are alternatingly tilted against each other. In this way, opposite weak TI surfaces are nonidentical, thereby providing the required interlayer coupling imbalance. This setup is extremely challenging but can be accomplished using terraces or creating trenches by, e.g., focused ion beams. The coupling between the layers can be fine tuned by varying the channel spacing, the channel width, and their relative angle. Finally, the channels must be filled with an insulating spacer material. The resulting sample can be viewed as a dimerized weak TI with a WSM layer on top of it. The characteristic features of the WSM, such as surface Fermi arcs, could be then detected by performing angle-resolved photoemission experiments.

TCI multilayer. The essential ingredient used in the setup above is the presence of two Dirac cones per surface which are coupled to each other. The question that arises is whether this idea is also applicable to systems in which surface Dirac cones are not pinned to TRI momenta. This occurs, for instance, in the recently discovered TCIs in the SnTe material class, which allows for an even number of *unpinned* surface Dirac cones protected by mirror symmetry [23].

TCIs are similar to "conventional" TIs except that topological states are protected by additional discrete symmetries, such as mirror, inversion, or space group symmetries [22,26,56–59]. For systems in the SnTe material class, this can be understood as follows: In the BZ of a mirror-symmetric material, there are planes that are invariant under the mirror operation M. Since the Bloch Hamiltonian $H(\mathbf{k})$ commutes with M in these planes, $H(\mathbf{k})$ can be brought in block form with respect to the mirror eigenvalues $\pm i$ of its eigenstates. For a mirror-invariant plane, we can assign a Chern number $n_{\pm i}$ to each of the two blocks. Furthermore, one can show that $n_{+i} = -n_{-i}$. Hence, $n_M = (n_{+i} - n_{-i})/2$ defines a $\mathbb{Z}$ topological invariant, the so-called mirror Chern number. In this sense, a TCI is a material with a nonzero mirror Chern number. By bulk-boundary correspondence, a nonzero mirror Chern number implies the presence of $|n_M|$ Dirac cones on surfaces which preserve the protecting mirror symmetry M [23].

In the remainder of this Rapid Communication, we are going to show that TCI multilayers also give rise to WSM phases. In analogy with weak TI heterostructures, let us consider a multilayer consisting of alternating layers of TCIs and OIs [see Fig. 3(a)]. Moreover, we will use a minimal TRI TCI with mirror Chern number $n_M = 2$ protected by a yz mirror plane. Thus, on surfaces parallel to the xy plane there will be two *unpinned* Dirac cones at momenta related by time-reversal symmetry. Without loss of generality, let them be at $\mathbf{k}_\perp = \pm \mathbf{d} = (0, \pm d)$. As opposed to a dimerized weak TI multilayer, the Dirac cones can be gapped even in the absence of intravalley scattering by breaking mirror symmetry with respect to the yz mirror plane. This can be accomplished, for instance, by a ferroelectric distortion [23,60]. Moreover, let
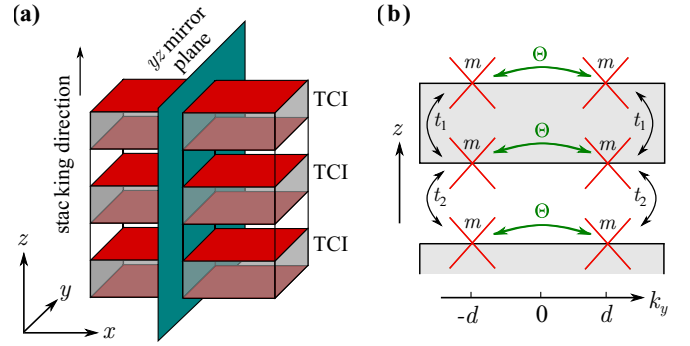

FIG. 3. TCI multilayer: (a) Cartoon of the multilayer design. The surfaces of the TCI layers (red) contribute two unpinned surface Dirac cones, each which is protected by a yz mirror plane. (b) Schematic of the coupling terms between the surface Dirac cones (red). The Dirac cones are connected by time reversal Θ and can be gapped by a mirror-symmetry breaking mass m.

the stacking direction of the TCI layers coincide with the z axis.

Taking into account a ferroelectric Dirac mass parametrized by m, which breaks the mirror symmetry of the system, the low-energy theory of the TCI multilayer can be written down in analogy with the weak TI heterostructure. The model parameters are illustrated in Fig. 3(b). The corresponding Hamiltonian is

$$\mathcal{H} = \sum_{\mathbf{k}_\perp, ij} \left[\frac{v_D}{2} \sigma^3 (\tau^0 + \tau^3)(\hat{z} \times \mathbf{s}) \cdot (\mathbf{k}_\perp + \mathbf{d}) \, \delta_{i,j} \right.$$
$$+ \frac{v_D}{2} \sigma^3 (\tau^0 - \tau^3)(\hat{z} \times \mathbf{s}) \cdot (\mathbf{k}_\perp - \mathbf{d}) \, \delta_{i,j}$$
$$+ t_1 \sigma^1 \tau^0 s^0 \, \delta_{i,j} + \frac{t_2}{2} (\sigma^- \delta_{i,j+1} + \sigma^+ \delta_{i,j-1}) \tau^0 s^0$$
$$\left. + m \, \sigma^0 \tau^3 s^3 \, \delta_{i,j} \right] c_{\mathbf{k}_\perp, j}^\dagger c_{\mathbf{k}_\perp, i}. \qquad (2)$$

The reflection operator is $M_x = i\sigma^0\tau^0 s^1$ with $k_x \to -k_x$. Time-reversal symmetry is preserved for all parameters with $\Theta = i\sigma^0\tau^1 s^2 K$, and $\mathbf{k} \to -\mathbf{k}$. The operator of spatial inversion is represented by $P = \sigma^1\tau^1 s^0$ (with $\mathbf{k} \to -\mathbf{k}$), and does not commute with the ferroelectric Dirac mass. Hence, the ferroelectric distortion also breaks inversion symmetry, which will enable us to create a stable WSM phase similar to the weak TI multilayer.

In Figs. 4(a) and 4(b), we show the t_1-t_2 phase diagrams of the heterostructure. For $m = 0$, the system preserves inversion symmetry. In this case, we find gapped phases for $t_1 \lessgtr t_2$, as well as a gapless phase along the line $t_1 = t_2$, as is shown in Fig. 4(a). In the latter, the system has two isolated bulk Dirac points at $\mathbf{k} = (0, \pm d, \pi)$.

For nonzero m, a WSM phase with four isolated Weyl points emerges in the phase diagram [see Fig. 4(b)]. The Weyl nodes have topological charges of ± 1. Furthermore, a new gapped phase appears around $(t_1, t_2) = (0,0)$.

Let us briefly comment on the gapped phases in Figs. 4(a) and 4(b). For $m \neq 0$, the point $(0,0)$ in the phase diagram represents a multilayer of decoupled, mirror-symmetry broken TCIs with gapped Dirac cones. This is a topologically trivial
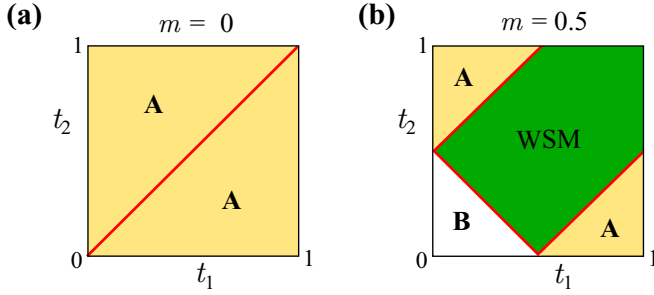
FIG. 4. Phase diagrams of the TCI multilayer with $v_D = 1$ and $\mathbf{d} = (0,1)$. (a) With inversion symmetry ($m = 0$): There are two gapped phases A (weak TI) and an unstable Dirac semimetal phase (red line). (b) Broken inversion symmetry ($m = 0.5$): A new gapped phase B (OI) emerges. Between the gapped phases there is a stable WSM phase (green) with four isolated Weyl points.

system. Hence, the B phase corresponds to a phase of OIs with $\mathbb{Z}_2$ invariants 0; (000). To determine the nature of the A phases, let us assume our model describes the low-energy theory of a lattice model. By analyzing how the parities change in the inversion-symmetric case ($m = 0$) by going from one A phase to the other, we find that both A phases are identical. For the inversion-symmetry broken case, let us consider the transition from the A phase to the B phase along the t_1 or along the t_2 axis. We observe that the bulk energy gap of the system closes along lines in momentum space at $(k_x, k_y) = (0, \pm d)$. Such a gap closing transition can only change the weak $\mathbb{Z}_2$ invariant v_3 relative to the B phase while the others remain unchanged. Hence, the A phases correspond to weak TIs with $\mathbb{Z}_2$ invariants 0; (001), i.e., their dark direction coincides with the stacking direction of the multilayer. We have verified this conclusion by comparing our results to a lattice regularization of our model (see Ref. [54]).

As opposed to the weak TI multilayer, the heterostructure based on TCI layers could be prepared in the form of a superlattice. The coupling between the surface Dirac cones can be adjusted by choosing a particular thickness for the layers of TCIs and OIs. To break mirror symmetry on the surfaces of the TCI layers, one could use an insulating, ferroelectric material for the layers in between the TCIs.

A concrete material candidate is a heterostructure of alternating layers of PbTe and SnTe stacked in the [110] direction [23]. SnTe is a TCI and hosts two Dirac cones on (110) surfaces protected by a $(1\bar{1}0)$ mirror plane, whereas PbTe is an OI. Moreover, SnTe undergoes a ferroelectric distortion at low temperatures [23]. The distortion is along the [111] direction. This breaks the $(1\bar{1}0)$ mirror plane, thereby providing an intrinsic mechanism to gap out the surface Dirac cones. Hence, this superlattice is expected to realize a WSM phase.

Conclusions. We have demonstrated that multilayer heterostructures based either on weak topological insulators or on topological crystalline insulators represent a different platform for the study of time-reversal invariant Weyl semimetals. In the proposed designs, thin layers of the materials are stacked on top of each other while inserting spacer layers of ordinary insulators in between. At the interfaces, pairs of pinned or unpinned Dirac cones, which are coupled to each other, provide the main ingredient of the multilayer designs. Weyl phases are stabilized by breaking inversion symmetry either by canting the interfaces or by a ferroelectric distortion.

We have shown that both design principles give rise to stable Weyl semimetal phases with four isolated Weyl points in the Brillouin zone. Moreover, the phase diagrams also indicate the possibility of strong topological insulator phases in the weak topological insulator multilayer, and of weak topological insulator phases in the topological crystalline insulator heterostructure. As a result, the multilayers may also provide a different way of designing artificial 3D topological insulators. Finally, we have given realistic pathways on how to prepare the proposed heterostructures by using available materials, such as $Bi_{13}Pt_3I_7$ or SnTe, and state-of-the-art technologies.

[1] X.-L. Qi and S.-C. Zhang, Rev. Mod. Phys. **83**, 1057 (2011).

[2] M. Z. Hasan and C. L. Kane, Rev. Mod. Phys. **82**, 3045 (2010).

[3] K. v. Klitzing, G. Dorda, and M. Pepper, Phys. Rev. Lett. **45**, 494 (1980).

[4] D. J. Thouless, M. Kohmoto, M. P. Nightingale, and M. den Nijs, Phys. Rev. Lett. **49**, 405 (1982).

[5] M. Sato and Y. Ando, Rep. Prog. Phys. **80**, 076501 (2017).

[6] V. Mourik, K. Zuo, S. M. Frolov, S. R. Plissard, E. P. A. M. Bakkers, and L. P. Kouwenhoven, Science **336**, 1003 (2012).

[7] A. A. Burkov, Nat. Mater. **15**, 1145 (2016).

[8] S. C. Zhang, Int. J. Mod. Phys. B **06**, 803 (1992).

[9] T. Senthil, Annu. Rev. Condens. Matter Phys. **6**, 299 (2015).

[10] M. Dzero, J. Xia, V. Galitski, and P. Coleman, Annu. Rev. Condens. Matter Phys. **7**, 249 (2016).

[11] A. Lau, C. Ortix, and J. van den Brink, Phys. Rev. Lett. **115**, 216805 (2015).

[12] C. L. Kane and E. J. Mele, Phys. Rev. Lett. **95**, 226801 (2005).

[13] L. Fu, C. L. Kane, and E. J. Mele, Phys. Rev. Lett. **98**, 106803 (2007).

[14] B. A. Bernevig, T. L. Hughes, and S.-C. Zhang, Science **314**, 1757 (2006).

[15] M. König, S. Wiedmann, C. Brüne, A. Roth, H. Buhmann, L. W. Molenkamp, X.-L. Qi, and S.-C. Zhang, Science **318**, 766 (2007).

[16] D. Hsieh, Y. Xia, L. Wray, D. Qian, A. Pal, J. H. Dil, J. Osterwalder, F. Meier, G. Bihlmayer, C. L. Kane, Y. S. Hor, R. J. Cava, and M. Z. Hasan, Science **323**, 919 (2009).

[17] Y. Xia, D. Qian, D. Hsieh, L. Wray, A. Pal, H. Lin, A. Bansil, D. Grauer, Y. S. Hor, R. J. Cava, and M. Z. Hasan, Nat. Phys. **5**, 398 (2009).

[18] B. Rasche, A. Isaeva, M. Ruck, S. Borisenko, V. Zabolotnyy, B. Büchner, K. Koepernik, C. Ortix, M. Richter, and J. van den Brink, Nat. Mater. **12**, 422 (2013).

[19] C. Pauly, B. Rasche, K. Koepernik, M. Liebmann, M. Pratzer, M. Richter, J. Kellner, M. Eschbach, B. Kaufmann, L. Plucinski, C. M. Schneider, M. Ruck, J. van den Brink, and M. Morgenstern, Nat. Phys. **11**, 338 (2015).

[20] C.-C. Liu, W. Feng, and Y. Yao, Phys. Rev. Lett. **107**, 076802 (2011).

[21] Y. Ando and L. Fu, Annu. Rev. Condens. Matter Phys. **6**, 361 (2015).

[22] L. Fu, Phys. Rev. Lett. **106**, 106802 (2011).

[23] T. H. Hsieh, H. Lin, J. Liu, W. Duan, A. Bansi, and L. Fu, Nat. Commun. **3**, 982 (2012).

[24] Y. Tanaka, Z. Ren, T. Sato, K. Nakayama, S. Souma, T. Takahashi, K. Segawa, and Y. Ando, Nat. Phys. **8**, 800 (2012).

[25] A. Alexandradinata, C. Fang, M. J. Gilbert, and B. A. Bernevig, Phys. Rev. Lett. **113**, 116403 (2014).

[26] A. Lau, J. van den Brink, and C. Ortix, Phys. Rev. B **94**, 165164 (2016).

[27] S. M. Young, S. Zaheer, J. C. Y. Teo, C. L. Kane, E. J. Mele, and A. M. Rappe, Phys. Rev. Lett. **108**, 140405 (2012).

[28] S. M. Young and C. L. Kane, Phys. Rev. Lett. **115**, 126803 (2015).

[29] K. Koepernik, D. Kasinathan, D. V. Efremov, S. Khim, S. Borisenko, B. Büchner, and J. van den Brink, Phys. Rev. B **93**, 201101(R) (2016).

[30] S.-M. Huang, S.-Y. Xu, I. Belopolski, C.-C. Lee, G. Chang, B. Wang, N. Alidoust, G. Bian, M. Neupane, C. Zhang, S. Jia, A. Bansil, H. Lin, and M. Z. Hasan, Nat. Commun. **6**, 7373 (2015).

[31] B. Q. Lv, H. M. Weng, B. B. Fu, X. P. Wang, H. Miao, J. Ma, P. Richard, X. C. Huang, L. X. Zhao, G. F. Chen, Z. Fang, X. Dai, T. Qian, and H. Ding, Phys. Rev. X **5**, 031013 (2015).

[32] B. Q. Lv, N. Xu, H. M. Weng, J. Z. Ma, P. Richard, X. C. Huang, L. X. Zhao, G. F. Chen, C. E. Matt, F. Bisti, V. N. Strocov, J. Mesot, Z. Fang, X. Dai, T. Qian, M. Shi, and H. Ding, Nat. Phys. **11**, 724 (2015).

[33] S.-Y. Xu, I. Belopolski, N. Alidoust, M. Neupane, G. Bian, C. Zhang, R. Sankar, G. Chang, Z. Yuan, C.-C. Lee, S.-M. Huang, H. Zheng, J. Ma, D. S. Sanchez, B. Wang, A. Bansil, F. Chou, P. P. Shibayev, H. Lin, S. Jia, and M. Z. Hasan, Science **349**, 613 (2015).

[34] S.-Y. Xu, N. Alidoust, I. Belopolski, Z. Yuan, G. Bian, T.-R. Chang, H. Zheng, V. N. Strocov, D. S. Sanchez, G. Chang, C.

Zhang, D. Mou, Y. Wu, L. Huang, C.-C. Lee, S.-M. Huang, B. Wang, A. Bansil, H.-T. Jeng, T. Neupert, A. Kaminski, H. Lin, S. Jia, and M. Z. Hasan, Nat. Phys. **11**, 748 (2015).

[35] H. Weng, C. Fang, B. A. Bernevig, and X. Dai, Phys. Rev. X **5**, 011029 (2015).

[36] E. Haubold, K. Koepernik, D. Efremov, S. Khim, A. Fedorov, Y. Kushnirenko, J. van den Brink, S. Wurmehl, B. Büchner, T. K. Kim, M. Hoesch, K. Sumida, K. Taguchi, T. Yoshikawa, A. Kimura, T. Okuda, and S. V. Borisenko, Phys. Rev. B **95**, 241108(R) (2017).

[37] X. Wan, A. M. Turner, A. Vishwanath, and S. Y. Savrasov, Phys. Rev. B **83**, 205101 (2011).

[38] A. A. Burkov and L. Balents, Phys. Rev. Lett. **107**, 127205 (2011).

[39] A. A. Zyuzin, S. Wu, and A. A. Burkov, Phys. Rev. B **85**, 165110 (2012).

[40] T. Ojanen, Phys. Rev. B **87**, 245112 (2013).

[41] A. A. Soluyanov, D. Gresch, Z. Wang, Q. Wu, M. Troyer, X. Dai, and B. A. Bernevig, Nature (London) **527**, 495 (2015).

[42] R. Okugawa and S. Murakami, Phys. Rev. B **89**, 235315 (2014).

[43] A. Lau, K. Koepernik, J. van den Brink, and C. Ortix, Phys. Rev. Lett. **119**, 076801 (2017).

[44] S. Juergens and B. Trauzettel, Phys. Rev. B **95**, 085313 (2017).

[45] G. C. Thiang, K. Sato, and K. Gomi, Nucl. Phys. B **923C**, 107 (2017).

[46] G. B. Halász and L. Balents, Phys. Rev. B **85**, 035103 (2012).

[47] M. R. Zirnbauer, J. Math. Phys. **37**, 4986 (1996).

[48] A. Altland and M. R. Zirnbauer, Phys. Rev. B **55**, 1142 (1997).

[49] S. Ryu, A. P. Schnyder, A. Furusaki, and A. W. W. Ludwig, New J. Phys. **12**, 065010 (2010).

[50] L. Fu and C. L. Kane, Phys. Rev. B **74**, 195312 (2006).

[51] A. Lau, C. Ortix, and J. van den Brink, Phys. Rev. B **91**, 085106 (2015).

[52] R. S. K. Mong, J. H. Bardarson, and J. E. Moore, Phys. Rev. Lett. **108**, 076804 (2012).

[53] L. Fu and C. L. Kane, Phys. Rev. B **76**, 045302 (2007).

[54] See Supplemental Material at http://link.aps.org/supplemental/ 10.1103/PhysRevB.96.081411, which includes Ref. [55], for studies of lattice regularizations based on the weak TI and TCI multilayer heterostructures.

[55] M. P. L. Sancho, J. M. L. Sancho, and J. Rubio, J. Phys. F **15**, 851 (1985).

[56] C.-K. Chiu, H. Yao, and S. Ryu, Phys. Rev. B **88**, 075142 (2013).

[57] K. Shiozaki and M. Sato, Phys. Rev. B **90**, 165114 (2014).

[58] T. L. Hughes, E. Prodan, and B. A. Bernevig, Phys. Rev. B **83**, 245132 (2011).

[59] R.-J. Slager, A. Mesaros, V. Juričić, and J. Zaanen, Nat. Phys. **9**, 98 (2012).

[60] J. W. F. Venderbos and L. Fu, Phys. Rev. B **93**, 195126 (2016).